Spatially Patterned Bi-electrode Epiretinal Stimulation for Axon Avoidance at Cellular Resolution

Ramandeep S. Vilkhu[1], Sasidhar S. Madugula[2], Lauren E. Grosberg[2], Alex R. Gogliettino[2], Pawel Hottowy[3], Wladyslaw Dabrowski[3], Alexander Sher[4], Alan M. Litke[4], Subhasish Mitra[1] & E.J. Chichilnisky[2]

[1] Department of Electrical Engineering, Stanford University, Stanford CA, USA. [2] Departments of Neurosurgery, Ophthalmology, and Hansen Experimental Physics Laboratory, Stanford University, Stanford CA, USA. [3] AGH University of Science and Technology, Faculty of Physics and Applied Computer Science, 30-059 Krakow, Poland. [4]Santa Cruz Institute for Particle Physics, University of California, Santa Cruz, CA, USA

Abstract

Objective. Epiretinal prostheses are designed to restore vision to people blinded by photoreceptor degenerative diseases by stimulating surviving retinal ganglion cells (RGCs), which carry visual signals to the brain. However, inadvertent stimulation of RGCs at their axons can result in non-focal visual percepts, limiting the quality of artificial vision. Theoretical work has suggested that axon activation can be avoided with current stimulation designed to minimize the second spatial derivative of the induced extracellular voltage along the axon. However, this approach has not been verified experimentally at the resolution of single cells. *Approach.* In this work, a custom multi-electrode array (512 electrodes, 10 μm diameter, 60 μm pitch) was used to stimulate and record RGCs in macaque retina *ex vivo* at single-cell, single-spike resolution. RGC activation thresholds resulting from bi-electrode stimulation, which consisted of bipolar currents simultaneously delivered through two electrodes straddling an axon, were compared to activation thresholds from traditional single-electrode stimulation. *Results.* Across three retinal preparations, the bi-electrode stimulation strategy reduced somatic activation thresholds while increasing axonal activation thresholds, thus favoring selective somatic activation. Furthermore, individual examples revealed rescued selective activation of somas that was not possible with any individual electrode. *Significance.* This work suggests that a bi-electrode epiretinal stimulation strategy can reduce inadvertent axonal activation at cellular resolution, for high-fidelity artificial vision.

Acknowledgements: This work was supported by the Stanford Graduate Fellowship (RSV), Research to Prevent Blindness Stein Innovation Award, Wu Tsai Neurosciences Institute Big Ideas, NIH NEI R01-EY021271, and NIH NEI P30-EY019005 (EJC), F30EY030776-03 (SSM), Polish National Science Centre Grant DEC-2013/10/M/NZ4/00268 (PH), AGH UST, task No. 11.11.220.01/4 within subsidy of the Ministry of Science and Higher Education (WD). We thank Jose Carmena, Mike Taffe, and the California National Primate Research Center for access to primate retinas, and Nishal Shah for useful discussions.

Keywords: retinal electrophysiology; retinal ganglion cells; epiretinal prosthesis; spatially-patterned stimulation strategy; cellular resolution; axon activation

Novelty & Significance: The effectiveness of bi-electrode stimulation for enhancing the electrical activation of retinal neurons was tested using high-density multi-electrode recording and stimulation in isolated macaque retina. The results suggest that spatially patterned bi-electrode stimuli reduce unwanted axon activation and thus improve the selectivity of stimulation at cellular resolution. Similar patterns could be implemented in a future high-resolution prosthesis to permit a more faithful replication of normal retinal activity, at the resolution of single-cells and single-spikes, for the treatment of incurable blindness.

Introduction

Epiretinal prostheses are designed to restore visual function in people blinded by photoreceptor degenerative diseases such as age-related macular degeneration or retinitis pigmentosa [1,2]. These devices are implanted on the retinal ganglion cell (RGC) side of the retina, and electrically activate RGCs that have survived the degeneration process, causing them to transmit artificial visual signals to the brain. Although devices implanted in patients have demonstrated some rudimentary vision restoration, the reported visual acuity and clinical value provided by existing devices is low [3–7].

One major problem limiting the visual acuity from existing epiretinal devices is the inadvertent activation of RGC axons [8,9]. In particular, activation of axons that originate from RGCs with visual receptive fields spatially distant from the location of electrical stimulation causes the perception of non-focal elongated phosphenes, limiting the quality of artificial vision [10].

In principle, selective activation of RGC somas while avoiding axons is possible with the use of effective temporal and spatial stimulation strategies, and several approaches have been proposed. Temporal stimulation strategies, which involve modulations of the stimulus waveform leading to maximally differentiable axon and somatic activations, include low frequency stimuli [11], cathodal monophasic pulsed stimuli [12], and charge-balanced long-duration bi-phasic pulsed stimuli [8]. Alternatively, spatial stimulation strategies leverage spatial biophysical activation characteristics of RGC axons to minimize axonal activation [13]. Examples of spatial strategies include rectangular electrodes positioned to straddle an axon [14,15] and patterned multi-electrode stimulation on a dense multi-electrode array [16].

While such approaches improve selective activation of RGC somas over axons to a degree, they fail to activate RGCs at the natural spatiotemporal resolution of the retina's neural code – single cells and single spikes. Specifically, a challenge for high-resolution epiretinal stimulation is the fact that different types of RGCs, each encoding unique aspects of the visual scene, are intermixed on the surface of the retina. Each RGC type signals visual information with precisely timed spikes that are highly stereotyped in all cells of each type. Hence, focal stimulation at the resolution of single cells and single spikes is likely required to reproduce high-fidelity vision. The temporal stimulation strategies discussed above depend on stimulus waveform modulations leading to network-mediated RGC activation, as opposed to direct RGC activation, and thus fail to match the temporal resolution of direct RGC activation (but see [17]). In contrast, the spatial stimulation strategies result in direct RGC activation, but the studies were either based in simulation or used experimental setups that failed to provide cellular and cell type resolution. Hence, it remains unclear whether such strategies can match the spatial resolution of the retina for use in a high-resolution epiretinal device.

Here, we test whether a biophysically-inspired spatial bi-electrode strategy can improve selectivity for stimulating RGC somas over axons at cellular resolution. Using large-scale, high-density recording and stimulation in isolated macaque retina [18–21], we evaluate how

effectively a given target RGC soma can be activated without activating a passing non-target axon, with both bi-electrode and single-electrode stimulation. In many cases across three retinal preparations, the bi-electrode strategy enhanced the selective activation of target RGC somas over non-target passing RGC axons. Furthermore, individual examples reveal rescued selective activation of somas that was not possible with any individual electrode, confirming the potential value of the approach for artificial vision.

Methods

Experimental setup

A custom 512-electrode system [18,21,22] was used to stimulate and record from RGCs in isolated rhesus macaque monkey (*Macaca mulatta*) retina. Retinas were obtained from terminally anesthetized animals euthanized during the course of research performed by other laboratories, which was conducted in accordance with institutional and national guidelines and regulations. Briefly, eyes were hemisected in room light following enucleation. Next, the vitreous was removed and the posterior portion of the eye containing the retina was kept in darkness in warm, oxygenated, bicarbonate buffered Ames' solution (Sigma). Patches of retina ~3 mm on a side were isolated under infrared light, placed RGC side down on the multielectrode array, and superfused with Ames solution at 35°C. Electrodes were 8-15 μm in diameter and arranged in a 16 × 32 isosceles triangular lattice with 60 μm spacing between adjacent electrodes [23]. Electrodes were electroplated with platinum. Voltage recordings were band-pass filtered between 43 and 5,000 Hz and sampled at 20 kHz. Spikes from individual RGCs in the voltage recordings were identified and sorted using standard spike sorting techniques [23].

Visual stimulation and cell type classification

To identify the type of each cell recorded, the retina was visually stimulated by a dynamic white noise stimulus, and the spike-triggered average (STA) stimulus was computed for each RGC, as previously described [24,25]. The STA summarizes the spatial, temporal, and chromatic structure of light response. In particular, clustering on the spatial (receptive field size) and temporal (time course) components of the STA was performed to identify distinct cell types, as previously described [26]. Analysis focused on ON and OFF parasol RGCs due to high SNR of their recorded spikes, which was useful for reliable spike sorting in the presence of electrical artifacts (see below).

Electrical image

The electrical image (EI) represents the average spatiotemporal pattern of voltage deflections produced on each electrode of the array during a spike from a given cell [23]. Electrical images for cells recorded on the array were calculated from data recorded during visual stimulation and

served as templates for the spike waveforms of the cells to be detected during electrical stimulation.

The spatial positions of relevant cell compartments (axon and soma) of a recorded cell relative to the electrode array were estimated using the electrical image. For each recorded cell, the shape of the spike waveform from the EI on an electrode was used for compartment identification: a triphasic waveform was taken to indicate recording from the cell axon whereas a biphasic waveform was taken to indicate recording from the cell soma [23]. Then, the temporal component of the EI was collapsed by computing the maximum negative amplitude over all electrodes. Using this purely spatial EI representation, a two-dimensional Gaussian was fitted over all electrodes recording somatic signals, to estimate the geometric area on the array electrically coupled to the soma, and a quadratic polynomial was fitted to all electrodes recording axonal signals, to estimate the axon trajectory (Fig. 1A) [27].

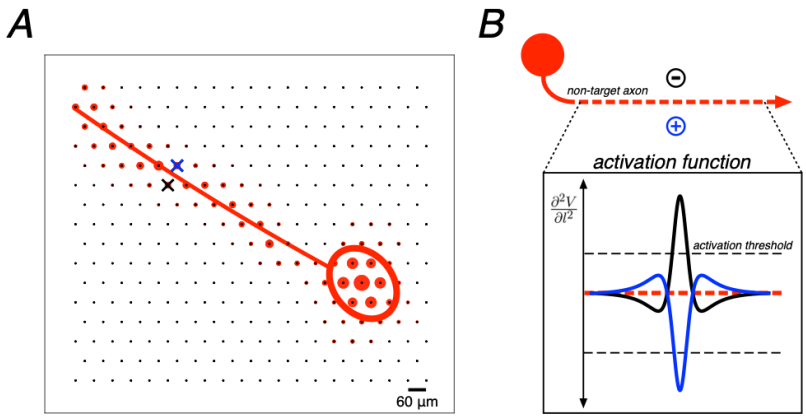

Figure 1. *Example electrical image decomposition into axonal and somatic compartments along with biophysical theory. A. Spatial component of the electrical image for a single cell plotted onto the electrode array. Size of the plotted circle represents relative strength of the signal, maximum negative amplitude of the electrical image on the electrode. Red line represents the quadratic spline fit to the axonal signals, corresponding to axon trajectory of the given cell, and the red ellipse represents the gaussian fit (2σ) to the somatic signals, corresponding to the geometric area on the array electrically coupled to the cell soma. Crosses represent an example bi-electrode stimulation pattern, straddling the axon fit (blue cross, positive polarity electrode; black cross, negative polarity electrode). B. Example of an ideal bi-electrode stimulus: a pair of electrodes perfectly straddling an axon while simultaneously active with fixed-ratio, opposite polarity currents. The resulting activation function, the second spatial derivative of voltage along the length of the axon, from each active electrode is shown: black curve from negative polarity electrode and blue curve from the positive polarity electrode. Since electric fields sum linearly over space, the resulting activation function from having both electrodes active simultaneously will be the sum of the two curves, cancelling out along the length of the axon.*

Electrical stimulation

Electrical stimulation was provided through one or more electrodes while recording RGC activity from all electrodes. Two types of stimulation patterns were tested: single-electrode stimulation

and bi-electrode stimulation. The single-electrode stimulation consisted of a charge-balanced, triphasic pulse passed through a single electrode. The triphasic pulse was composed of anodal/cathodal/anodal phases with relative current amplitudes 2:-3:1 and phase duration of 50 μs per phase (150 μs total). These parameters were chosen to minimize the electrical artifact [18,19,21]. Single electrode stimulation was delivered in 25 repeated trials at 40 current amplitudes (10% increments) between 0.1 and 3.7 μA. The bi-electrode stimulation consisted of the same single-electrode current pattern passed through one electrode, but with equal and opposite-polarity current simultaneously passed through an adjacent electrode. The stimulating electrodes were chosen based on highest SNR of recorded spikes and the electrodes were spatially patterned such that the pair of simultaneously active electrodes straddled a passing axon, as estimated by the fitted axon trajectory (see above), to minimize the activation function along the length of the axon [10,20] (Fig. 1B). Bi-electrode stimulation was supplied for multiple trials at varying current amplitudes (10% increments) between 0.2 and 3.8 μA (retina 1; 40 repetitions), 0.2 and 4.9 μA (retina 2; 20 repetitions), or 0.2 and 4.3 μA (retina 3; 25 repetitions). The ordering of the stimulation patterns was chosen pseudo-randomly, restricted so that each successive stimulating electrode or pair of electrodes was far from the previous and subsequent stimulating electrodes. This was done to avoid stimulating the same cell(s) in rapid succession.

Responses to electrical stimulation

The spikes recorded during electrical stimulation were analyzed using a custom supervised template matching method [19]. Briefly, an automated algorithm separated spikes from the electrical artifact by grouping traces according to an estimated artifact waveform (scaled voltage waveform recorded at low amplitudes, which contained no spikes or only spontaneous spikes) and the average recorded spike waveform from visual stimulation, i.e. the electrical image (see above). Specifically, the artifact waveform estimate at each stimulation amplitude was subtracted from spiking trials to yield an artifact-subtracted spike waveform, which was compared against the electrical image. The electrical image and electrical artifact-subtracted spike waveform templates were visually inspected for sorting errors and manually corrected as needed.

For each analyzed cell, spike probabilities were calculated across 20-40 trials at each stimulus current amplitude, and cell spiking probability was modeled as a function of current amplitude by a sigmoidal relationship (Equation 1).

$$p(a) = \frac{1}{1 + e^{-k(a-b)}} \tag{1}$$

where a is the current amplitude, p(a) is the spike probability of a given cell, and k and b are free parameters (representing sigmoidal slope and threshold, respectively). Fitted sigmoidal curves were used to compute the *activation threshold*, defined as the current amplitude producing 50 percent spiking probability.

Statistical analysis of threshold and selectivity changes

The relationship between activation thresholds obtained from bi-electrode and single electrode stimulation was analyzed using a resampling approach. To determine the estimated variation in the slopes of lines fitted in Fig. 2 and Fig. 3, data were resampled with replacement, producing simulated data sets with the same number of points as the real data set, drawn from the distribution given by the measured data. This resampling was repeated 1000 times and, for each iteration of resampling, the slope of the least squares linear fit to the data was computed. Values in the text correspond to the slope values obtained from the measured data along with 90% confidence intervals based on the resampled data.

Results

Electrical recording and stimulation were performed on isolated macaque retinas using a high-density 512-electrode array (see Methods). Direct RGC activation caused by current pulses passed through one or two electrodes simultaneously was investigated based on biophysically derived insight into the mechanism of axonal activation [13,29]. To determine the effectiveness of bi-electrode stimulation to selectively activate cells, stimulation of a target soma and a non-target axon with a single electrode on one side of the axon was compared to bi-electrode stimulation with an equal and opposite current pulse simultaneously through a second electrode on the opposite side of the axon.

After delivering 20-40 current pulses (triphasic, charge-balanced, 50 μs per phase, 150 μs total duration) at 30-40 current levels, a sigmoidal relationship was used to characterize the probability of RGC activation as a function of injected current. The current amplitude level corresponding to RGC activation on 50% of stimulation trials was estimated and defined as the *activation threshold* (see Methods). Stimulation was performed near the soma of a target RGC and near the axon of a non-target RGC using information from the recorded electrical images (EIs) of the cells. The EI represents the average spatiotemporal pattern of voltage deflections produced on each electrode of the array during a spike from a given cell (see Methods). Somatic or axonal stimulation was achieved by using the EIs to determine electrodes that recorded unambiguous somatic (biphasic) or axonal (triphasic) spikes from the target RGC soma or the non-target RGC axon, respectively [23]. To determine the position and orientation of the axon with respect to the stimulating electrodes, a quadratic spline was fitted to interpolate the trajectory of the axonal compartment of the electrical image [27].

Effect of bi-electrode strategy on somatic and axonal RGC activation thresholds

Comparison of thresholds obtained with single-electrode and bi-electrode stimulation revealed two trends. First, as predicted, bi-electrode stimulation systematically increased axonal thresholds (Fig. 2). Second, on average, bi-electrode stimulation decreased somatic thresholds, however, there was noticeable variability in the observed threshold changes (see Discussion) (Fig. 2). To quantify the relationship between bi-electrode and single-electrode stimulation of

axons and somas across retinas, the slopes of the relation between bi-electrode and single-electrode activation thresholds (Fig. 2) were computed, along with 90% confidence intervals on the slope obtained by resampling (see Methods; Table 1). For cells activated at somatic compartments (grey points, Fig. 2), on average, bi-electrode stimulation resulted in lower thresholds than single-electrode stimulation (slopes below 1) in all three retinas. In contrast, for cells activated at axonal compartments (red points, Fig. 2), bi-electrode stimulation produced higher thresholds compared to single-electrode stimulation in all three retinas. These overall trends suggest that bi-electrode stimulation could be used to selectively activate somas over axons.

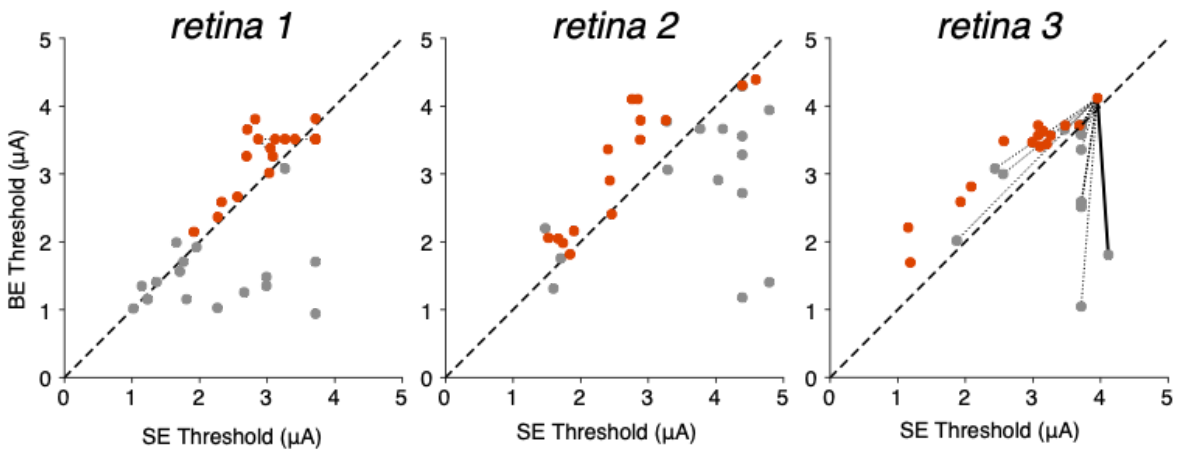

Figure 2. *Axonal and somatic activation thresholds from bi-electrode stimulation and single-electrode stimulation.* Scatter plots for three different preparations show activation threshold of analyzed cells to bi-electrode (BE) and single-electrode (SE) stimulation. Grey diagonals denote the reference line y = x. Grey points indicate somas and red points indicate axons. An example of the method used to calculate predicted improvement in selectivity (see Fig. 3) is illustrated in retina 3: dashed lines show all possible surrogate pairings between a non-target axon (single red point) and all somas (grey points); solid line denotes a soma-axon pair targeted by the same set of electrodes. Data are shown from 40 distinct cells, 192 distinct cell-electrode pairs across the three retinal preparations.

Table 1. *Change in axon and soma activation thresholds with bi-electrode vs single-electrode stimulation*. Columns of the table represent RGCs activated at somatic compartments versus RGCs activated at axonal compartments (somas and axons). Each entry indicates the fitted slope of the data in Fig. 2, with 90% confidence intervals on the slope obtained by resampling with replacement 1000 times (see Methods). The last row shows the aggregate statistics from all cells across all three retinas.

BE vs. SE thresholds *mean (90% confidence interval)*		
	somas	axons
retina 1	0.71 (0.59, 0.83) n = 18	1.08 (1.04, 1.13) n = 18
retina 2	0.76 (0.64, 0.87) n = 15	1.22 (1.13, 1.31) n = 15
retina 3	0.86 (0.74, 0.97) n = 15	1.17 (1.12, 1.25) n = 15
pooled	0.79 (0.72, 0.86) n = 48	1.14 (1.10, 1.18) n = 48

Bi-electrode strategy enhances selective activation of target soma over non-target axon

It is unclear from the thresholds alone how useful the strategy will be in real scenarios of a single axon passing by a target soma. To test the usefulness of the approach, specific instances of selective activation of target somas over nearby non-target axons were examined. The target soma and non-target axon were stimulated by the same electrode or pair of electrodes using single-electrode or bi-electrode stimulation, respectively. *Selectivity*, defined as the ratio of non-target axon activation threshold to target soma activation threshold, was computed for both bi-electrode and single-electrode stimulation. The selectivity for activating a target soma over a non-target axon was systematically higher for bi-electrode stimulation versus single-electrode stimulation in all three retinas (Fig. 3, open symbols).

In the above analysis, the number of soma-axon pairs stimulated by the same pair of electrodes was limited by the difficulty of reliably spike sorting the cell response to electrical stimulation. Therefore, a surrogate analysis was also performed, comparing the activation thresholds of all pairs of somas and axons in the same retina (Fig. 2, surrogate analysis visual). In this analysis, the target soma and non-target axon were in fact stimulated by different electrodes on the array, but the increased number of analyzable pairs served to increase the statistical power of the single-electrode vs. bi-electrode comparison. Selectivity was systematically higher with bi-electrode stimulation (Fig. 3). Slopes fitted to these data, along with 90% confidence intervals on the slope obtained by resampling (see Methods), confirmed the trend in all three retinas and in the data pooled across retinas (Table 2).

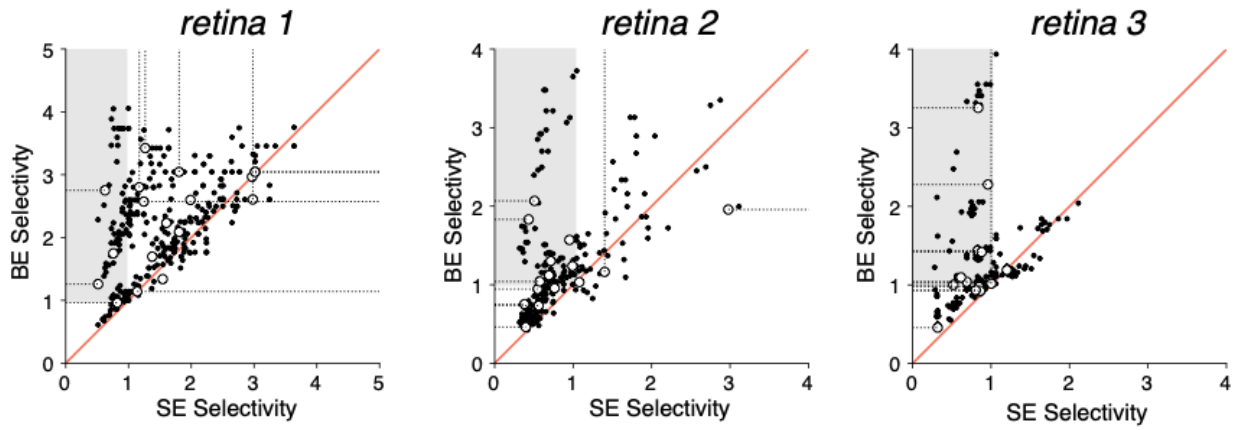

Figure 3. *Impact of bi-electrode stimulation strategy on selectivity.* Scatter plots with each point representing selectivity calculated for a target soma (grey points from Fig. 2) and non-target axon (red points from Fig. 2) pair with bi-electrode (BE) and single-electrode (SE) stimulation in three retinas. Red diagonals denote the reference line y = x. Selectivity is defined as the ratio of non-target axon threshold to target soma threshold. Open and closed symbols represent true (soma-axon pairs stimulated with the same set of electrodes) and surrogate pairings, respectively. Shaded region represents regions of rescued selectivity (Fig. 4). Open symbols with dotted tails represent scenarios where the target soma or non-target axon did not spike even at the maximum supplied current amplitude, so selectivity was calculated with the threshold set to the largest current amplitude tested, and the tail shows the hypothetical change in selectivity for larger thresholds.

Table 2. *Change in selectivity with bi-electrode vs single-electrode stimulation*. Each entry indicates the fitted slope of the bi-electrode versus single electrode selectivity data from Fig. 3, with 90% confidence intervals on the slope obtained by resampling from the data with replacement 1000 times (see Methods). The last row indicates the aggregate results from all cells across all three retinas.

Selectivity measured by thresholds mean (90% confidence interval)	
	bi-electrode vs single electrode
retina 1	1.43 (1.37, 1.49)
retina 2	1.54 (1.44, 1.64)
retina 3	1.48 (1.40, 1.57)
pooled	1.46 (1.42, 1.50)

Rescued selectivity

In some cases, bi-electrode stimulation made it possible to selectively activate a soma that could not be selectively activated with any nearby individual electrode (three examples shown in

Fig. 4). Specifically, in many soma-axon pairs recorded on the same electrodes (n = 29), it was not possible to selectively activate the soma without unwanted axonal activation of a distant cell using the electrodes near the cell (SE selectivity < 1; Fig. 3). However, in a majority of cases (18/29), bi-electrode stimulation resulted in selective activation of the soma without activation of the axon, rescuing selectivity (BE selectivity > 1; Fig. 3 shaded region).

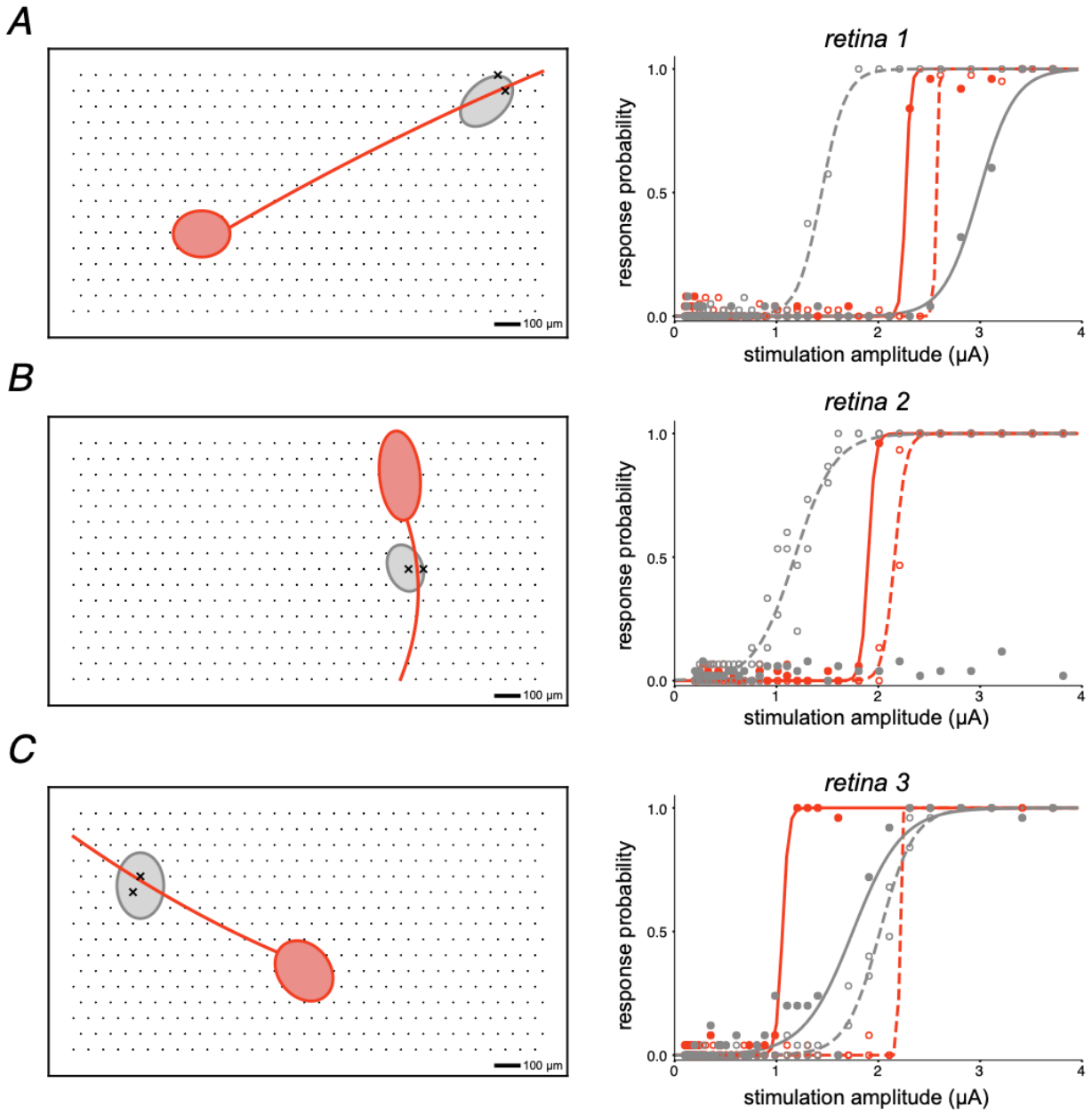

Figure 4. *Electrical images and activation curves for target somas and non-target axons exhibiting rescued selectivity.* Each panel on the left corresponds to simplified electrical images of axonal and somatic compartments of recorded parasol cells over a region of the electrode array, shown by fitting elliptical Gaussians to the somatic compartment of the cells and a quadratic spline to the axonal compartment (see Methods). Soma-axon pairs A, B, and C were from retina 1, 2, and 3, respectively. Each soma-axon pair was stimulated with the same electrode(s) with single-electrode and bi-electrode

stimulation, respectively. The activation curves for each soma-axon pair are shown in the right column. Solid lines indicate response to single electrode stimulation; dashed lines indicate response to bi-electrode stimulation. Red curves represent the response of the non-target axon; grey curves represent the response of the target soma. In all cases, bi-electrode stimulation shifted the non-target axon (red) activation probability curve to the right, resulting in a higher activation threshold relative to single electrode stimulation. In A, bi-electrode stimulation shifted the target soma (grey) activation probability curve to the left, resulting in a lower activation threshold. In B, the target soma did not respond to the single electrode stimulation current range tested, but responded to bi-electrode stimulation, resulting in an activation probability curve. In C, bi-electrode stimulation shifted the target soma activation probability curve to the right, resulting in a higher activation threshold, but the relative change in the non-target axon activation curves still resulted in rescued selectivity.

Discussion

The results indicate that bi-electrode stimulation can enhance the selectivity of stimulating RGC somas over axons in the primate retina (Fig. 3). Furthermore, bi-electrode selectivity improvements were demonstrated by individual scenarios in which a specific soma could be effectively activated without activation of a specific nearby axon, in a way that was not possible with the individual electrodes of the array (Fig. 4). This is significant because activation of a distant cell, encoding a distant region of the visual field, at its axon can cause unwanted visual information to be transmitted to the brain [10]. These findings are consistent with previous simulation and experimental work [14–16]. The primary novel aspect of the present study is that RGC activation was probed at the natural spatiotemporal resolution of the retinal code -- single cells and single spikes -- which may be important for high-fidelity artificial vision with future clinical implants.

Jensen et al. [17] proposed another mechanism for selective somatic activation in the retina using short-duration pulsed stimuli. While the study showed differentiable somatic and axonal activation thresholds the data were independently gathered for spatially distant axons and somas, not simultaneously for overlapping somas and axons. Furthermore, other studies performed with many cells and retinas have demonstrated that short-duration stimulation leads to significant inadvertent axon activation [21,30,31].

Although axonal thresholds increased with bi-electrode stimulation, somatic thresholds sometimes increased and sometimes decreased (Fig 2). A possible explanation is that the secondary electrode deflects current flow in a direction either towards or away from excitable cell structures (e.g., the axon initial segment) [19,32–35] depending on the geometry of the electrodes relative to the cell. A related possibility is that current is deflected toward or away from multiple activation sites, non-linearly modifying the probability of activation [36]. While these hypotheses deserve further examination, the overall trend was that bi-electrode stimulation enhanced selectivity significantly in spite of somatic threshold variability.

The cell types examined in this study were ON and OFF parasol cells, two numerically dominant cell types in primates (~16% of the RGC population [37]), in the peripheral retina. A major reason for this focus is that the large spikes produced by these cells were comparatively easy to identify in the presence of the electrical stimulation artifact. However, other cell types (e.g., midget cells: comprising ~50% of the RGC population) must be investigated in the future for a more comprehensive study of the efficacy of bi-electrode stimulation. Furthermore, future devices target implantation in more central regions of the retina (e.g., the raphe) to enable the highest resolution artificial vision, and the bi-electrode strategy has yet to be investigated in these regions. Additionally, the analysis focused on the relative threshold changes of a single target cell and single non-target cell, ignoring other cells near the stimulation site(s). In reality, threshold changes in all nearby cells must be accounted for to comprehensively determine the selectivity improvement from bi-electrode stimulation. However, it was difficult to investigate threshold changes for many non-target cells because the process of manually sorting spikes after electrical stimulation is time-consuming [19,21]. One potential solution would be the development of algorithms to automate spike sorting in the presence of electrical artifacts, particularly for multi-electrode stimulation, an effort that is underway [38].

The biophysical motivation of the bi-electrode strategy is that it decreases the magnitude of the induced electric field along the longitudinal direction of an axon, resulting in decreased axon activation. However, the electric field near the stimulating electrodes will vary with different stimulation hardware geometries. The present work tested this strategy on a 60 μm pitch electrode array with ~10 μm diameter electrodes. Variations in electrode size, pitch, and shape would likely result in variations of the induced electric field along the axon, and thus variation in activation thresholds. Although exploration of novel electrodes could further improve axon suppression through tailored electric field shaping, such changes could impact the ability to focally stimulate cells. For example, long rectangular electrodes have been shown to shape electric fields in a manner that minimizes axon activation [14,15]. However, long electrodes are not ideal for focal stimulation of single cells due to current spread. The densely packed triangular lattice electrode arrangement in this study has the advantage of flexibility: such a hardware geometry could be used to provide high density single electrode stimulation, while at the same time allowing some of the advantages of axon avoidance with bi-electrode stimulation.

These findings suggest that bi-electrode stimulation can improve the performance of next-generation epiretinal prostheses designed to operate at single cell resolution. Practically, a future device would determine the amplitude of current that must be passed through a given electrode to selectively activate a RGC, create such a mapping for all cell-electrode pairs across the array, and implement an electrical stimulation strategy based on these data to optimize artificial vision [39]. For cases in which a cell is not selectively activatable with a single electrode due to inadvertent activation of a distant RGC at its axon, the device would supply the bi-electrode stimulus to minimize the probability of axonal activation. Thus, the strategy presented here has the potential to mitigate a long-standing problem for epiretinal prosthetic devices.

References

1. Ferris FL 3rd, Fine SL, Hyman L. Age-related macular degeneration and blindness due to neovascular maculopathy. Arch Ophthalmol. 1984;102: 1640–1642.

2. Phelan JK, Bok D. A brief review of retinitis pigmentosa and the identified retinitis pigmentosa genes. Mol Vis. 2000;6: 116–124.

3. Humayun MS, de Juan E Jr, Dagnelie G, Greenberg RJ, Propst RH, Phillips DH. Visual perception elicited by electrical stimulation of retina in blind humans. Arch Ophthalmol. 1996;114: 40–46.

4. Rizzo JF 3rd, Wyatt J, Loewenstein J, Kelly S, Shire D. Perceptual efficacy of electrical stimulation of human retina with a microelectrode array during short-term surgical trials. Invest Ophthalmol Vis Sci. 2003;44: 5362–5369.

5. Weiland JD, Humayun MS. Retinal prosthesis. IEEE Trans Biomed Eng. 2014;61: 1412–1424.

6. Hadjinicolaou AE, Meffin H, Maturana MI, Cloherty SL, Ibbotson MR. Prosthetic vision: devices, patient outcomes and retinal research. Clin Exp Optom. 2015;98: 395–410.

7. Zrenner E, Bartz-Schmidt KU, Benav H, Besch D, Bruckmann A, Gabel V-P, et al. Subretinal electronic chips allow blind patients to read letters and combine them to words. Proc Biol Sci. 2011;278: 1489–1497.

8. Weitz AC, Nanduri D, Behrend MR, Gonzalez-Calle A, Greenberg RJ, Humayun MS, et al. Improving the spatial resolution of epiretinal implants by increasing stimulus pulse duration. Sci Transl Med. 2015;7: 318ra203.

9. Nanduri D, Fine I, Horsager A, Boynton GM, Humayun MS, Greenberg RJ, et al. Frequency and amplitude modulation have different effects on the percepts elicited by retinal stimulation. Invest Ophthalmol Vis Sci. 2012;53: 205–214.

10. Beyeler M, Nanduri D, Weiland JD, Rokem A, Boynton GM, Fine I. A model of ganglion axon pathways accounts for percepts elicited by retinal implants. Sci Rep. 2019;9: 9199.

11. Fried SI, Freeman DK, Rizzo JF. Low Frequency Sinusoids Avoid Axonal Stimulation With Retinal Prosthetics. Invest Ophthalmol Vis Sci. 2010;51: 4318–4318.

12. Jensen RJ, Rizzo JF 3rd, Ziv OR, Grumet A, Wyatt J. Thresholds for activation of rabbit retinal ganglion cells with an ultrafine, extracellular microelectrode. Invest Ophthalmol Vis Sci. 2003;44: 3533–3543.

13. Rattay F. The basic mechanism for the electrical stimulation of the nervous system. Neuroscience. 1999. pp. 335–346. doi:10.1016/s0306-4522(98)00330-3

14. Tong W, Hejazi M, Garrett DJ, Esler T, Prawer S, Meffin H, et al. Minimizing axon bundle activation of retinal ganglion cells with oriented rectangular electrodes. J Neural Eng. 2020;17: 036016.

15. Rattay F, Resatz S. Effective electrode configuration for selective stimulation with inner eye prostheses. IEEE Trans Biomed Eng. 2004;51: 1659–1664.

16. Esler TB, Kerr RR, Tahayori B, Grayden DB, Meffin H, Burkitt AN. Minimizing activation of overlying axons with epiretinal stimulation: The role of fiber orientation and electrode configuration. PLOS ONE. 2018. p. e0193598. doi:10.1371/journal.pone.0193598

17. Jensen RJ, Ziv OR, Rizzo JF 3rd. Thresholds for activation of rabbit retinal ganglion cells with

relatively large, extracellular microelectrodes. Invest Ophthalmol Vis Sci. 2005;46: 1486–1496.

18. Hottowy P, Skoczeń A, Gunning DE, Kachiguine S, Mathieson K, Sher A, et al. Properties and application of a multichannel integrated circuit for low-artifact, patterned electrical stimulation of neural tissue. J Neural Eng. 2012;9: 066005.

19. Jepson LH, Hottowy P, Mathieson K, Gunning DE, Dabrowski W, Litke AM, et al. Focal electrical stimulation of major ganglion cell types in the primate retina for the design of visual prostheses. J Neurosci. 2013;33: 7194–7205.

20. Jepson LH, Hottowy P, Weiner GA, Dabrowski W, Litke AM, Chichilnisky EJ. High-fidelity reproduction of spatiotemporal visual signals for retinal prosthesis. Neuron. 2014;83: 87–92.

21. Grosberg LE, Ganesan K, Goetz GA, Madugula SS, Bhaskhar N, Fan V, et al. Activation of ganglion cells and axon bundles using epiretinal electrical stimulation. J Neurophysiol. 2017;118: 1457–1471.

22. Hottowy P, Dąbrowski W, Skoczeń A, Wiącek P. An integrated multichannel waveform generator for large-scale spatio-temporal stimulation of neural tissue. Analog Integrated Circuits and Signal Processing. 2008;55: 239–248.

23. Litke AM, Bezayiff N, Chichilnisky EJ, Cunningham W, Dabrowski W, Grillo AA, et al. What does the eye tell the brain?: Development of a system for the large-scale recording of retinal output activity. IEEE Trans Nucl Sci. 2004;51: 1434–1440.

24. Chichilnisky EJ. A simple white noise analysis of neuronal light responses. Network: Computation in Neural Systems. 2001. pp. 199–213. doi:10.1080/713663221

25. Chichilnisky EJ, Kalmar RS. Functional asymmetries in ON and OFF ganglion cells of primate retina. J Neurosci. 2002;22: 2737–2747.

26. Field GD, Sher A, Gauthier JL, Greschner M, Shlens J, Litke AM, et al. Spatial properties and functional organization of small bistratified ganglion cells in primate retina. J Neurosci. 2007;27: 13261–13272.

27. Li PH, Gauthier JL, Schiff M, Sher A, Ahn D, Field GD, et al. Anatomical identification of extracellularly recorded cells in large-scale multielectrode recordings. J Neurosci. 2015;35: 4663–4675.

28. Front Matter. The Jackknife, the Bootstrap and Other Resampling Plans. Society for Industrial and Applied Mathematics; 1982. pp. i–xi. doi:10.1137/1.9781611970319.fm

29. Eickenscheidt M, Zeck G. Action potentials in retinal ganglion cells are initiated at the site of maximal curvature of the extracellular potential. J Neural Eng. 2014;11: 036006.

30. Boinagrov D, Pangratz-Fuehrer S, Goetz G, Palanker D. Selectivity of direct and network-mediated stimulation of the retinal ganglion cells with epi-, sub- and intraretinal electrodes. J Neural Eng. 2014;11: 026008.

31. Boinagrov D, Loudin J, Palanker D. Strength–Duration Relationship for Extracellular Neural Stimulation: Numerical and Analytical Models. J Neurophysiol. 2010;104: 2236–2248.

32. Matteucci PB, Chen SC, Tsai D, Dodds CWD, Dokos S, Morley JW, et al. Current steering in retinal stimulation via a quasimonopolar stimulation paradigm. Invest Ophthalmol Vis Sci. 2013;54: 4307–4320.

33. Dumm G, Fallon JB, Williams CE, Shivdasani MN. Virtual electrodes by current steering in retinal

prostheses. Invest Ophthalmol Vis Sci. 2014;55: 8077–8085.

34. Fan VH, Grosberg LE, Madugula SS, Hottowy P, Dabrowski W, Sher A, et al. Epiretinal stimulation with local returns enhances selectivity at cellular resolution. J Neural Eng. 2019;16: 025001.

35. Bareket L, Barriga-Rivera A, Zapf MP, Lovell NH, Suaning GJ. Progress in artificial vision through suprachoroidal retinal implants. J Neural Eng. 2017;14: 045002.

36. Jepson LH, Hottowy P, Mathieson K, Gunning DE, Dąbrowski W, Litke AM, et al. Spatially patterned electrical stimulation to enhance resolution of retinal prostheses. J Neurosci. 2014;34: 4871–4881.

37. Dacey DM. Origins of perception: retinal ganglion cell diversity and the creation of parallel visual pathways. The cognitive neurosciences. 2004;3: 281–301.

38. Mena GE, Grosberg LE, Madugula S, Hottowy P, Litke A, Cunningham J, et al. Electrical stimulus artifact cancellation and neural spike detection on large multi-electrode arrays. PLoS Comput Biol. 2017;13: e1005842.

39. Shah N, Madugula S, Hottowy P, Sher A, Litke A, Paninski L, et al. Efficient characterization of electrically evoked responses for neural interfaces. Adv Neural Inf Process Syst. 2019;32: 14444–14458.